Photon Lasers Med 1 (2012): 103–115 © 2012 by Walter de Gruyter • Berlin • Boston. DOI 10.1515/plm-2012-0006

A low-cost needle-based single-fiber reflectance spectroscopy method to probe scattering changes associated with mineralization in intervertebral discs in chondrodystrophoid canine species – A pilot study

Untersuchung des Zusammenhangs zwischen Mineralisationsgrad und Rückstreuverhalten in Bandscheiben bei chondrodystrophen Hunderassen – Eine Pilotstudie zur Anwendbarkeit einer kostengünstigen, nadelbasierten Einzelfaser-Spektroskopie-Methode

Daqing Piao[1,*], Kelci McKeirnan[2], Yuanyuan Jiang[1], Melanie A. Breshears[3] and Kenneth E. Bartels[2]

[1] School of Electrical and Computer Engineering, Oklahoma State University, 202 Engineering South, Stillwater, OK 74078, USA, e-mail: daqing.piao@okstate.edu
[2] Department of Veterinary Clinical Science and Veterinary Surgical Laser Laboratory, Center for Veterinary Health Sciences, Farm Road, Oklahoma State University, Stillwater, OK 74078, USA
[3] Department of Veterinary Pathobiology, Oklahoma State University, 250 McElroy Hall, Stillwater, OK 74078, USA

*Corresponding author

Abstract

Background and objectives: Intervertebral disc herniation is a common disease in chondrodystrophic dogs, and a similar neurologic condition also occurs in humans. Percutaneous laser disc ablation (PLDA) is a minimally invasive procedure used increasingly for prevention of disc herniation. PLDA is performed on thoracolumbar discs to which the same laser energy is applied regardless of their mineral content. Knowledge of individual disc mineral composition would allow laser energy dosage adjustments and more accurate treatment of degenerative discs. Usually, PLDA is guided by radiography/fluoroscopy, which has a limited sensitivity of approximately 60% for identification of mineralized discs. An imaging or sensing technology that provides a more accurate pre-operative *in-situ* assessment of the disc mineralization, and potentially rapid post-operative feedback, could optimize the outcome of the PLDA procedure. A sensing technology of needle-probing single-fiber reflectance (SFR) spectroscopy is therefore proposed that is considered to be compatible with PLDA work flow. The objective of this study was to demonstrate the feasibility of this technology in assessing the increased light scattering associated with mineralization in intervertebral discs in chondrodystrophoid canine species.
Materials and methods: A pilot study was performed on a total of 21 intervertebral discs from two cadaveric dogs ("Dog A" and "Dog B"). The discs were imaged by computed tomography (CT), radiography, and SFR spectroscopy, before histopathologic examination. SFR spectroscopy in the visible/near-infrared band was performed on the nucleus pulposus of the intervertebral disc through a 20-gauge spinal needle placed percutaneously for PLDA. A normalization method was applied to the raw remission spectra to extract a dimension-less and wavelength-dependent intensity profile in the 500–950 nm spectral range.
Results: In total, six discs were determined to be degenerative on histopathology, five discs of "Dog A" and one disc of "Dog B". CT diagnosed all six degenerated discs, whereas radiography missed two of the five degenerated discs of "Dog A". The wavelength-dependent mean scattering intensity profiles of the six degenerated discs were noticeably higher than the mean scattering intensity profiles of the 15 "normal" or insignificantly mineralized discs over the entire spectral range. The mean scattering intensities, averaged over each of the entire profiles, were 2.79±0.58 (mean±SD) for the six degenerated discs and 1.48±0.37 for the 15 "normal" or insignificantly mineralized discs. A two-sample *t*-test showed $p<0.001$ for the difference of the averaged scattering intensity between these both groups of discs.
Conclusions: SFR spectroscopy measurements indicate that the increase of light scattering intensity across the entire 500–950 nm spectral range is associated with the mineralization in canine intervertebral discs. However, the scattering characteristics of the nucleus pulposus measured in this study may not necessarily represent the optical properties of the nucleus pulposus at the laser wavelength used for PLDA (2100 nm). More studies on cadaveric and eventually *in-vivo* samples are necessary before the clinical feasibility can be proved.

Keywords: intervertebral disc degeneration; single-fiber reflectance spectroscopy; scattering; percutaneous laser disc ablation.

Zusammenfassung

Hintergrund und Zielsetzung: Der Bandscheibenvorfall tritt häufig bei chondrodystrophen Hunderassen auf und ist

mit der neurologischen Erkrankung bei Menschen vergleichbar. Die perkutane Laserablation der Bandscheibe (percutaneous laser disc ablation, PLDA) ist eine minimal-invasive Prozedur, die zunehmend präventiv eingesetzt wird. Dabei wird Laserlicht gleicher Energiedichte in die Bandscheiben im Übergangsbereich der Brust- zur Lendenwirbelsäule appliziert, unabhängig von deren Mineralgehalt. Die genaue Kenntnis des individuellen Mineralisationsgrades jeder Bandscheibe könnte helfen, die Laserenergie besser zu justieren und die degenerierten Bandscheiben effektiver zu behandeln. Normalerweise wird die PLDA-Prozedur mittels Radiographie/Fluoroskopie überwacht, allerdings liegt die Sensitivität hier nur bei 60%. Ein Monitoring- oder Sensorverfahren, das sowohl die präoperative Bestimmung des Mineralgehalts der jeweiligen Bandscheibe erlaubt als auch ein schnelles post-operatives Feedback liefert, könnte den Behandlungserfolg der PLDA verbessern. Daher wurde ein kostengünstiger, punktionsnadel-basierter Ansatz zur Erfassung der Rückstreuung verfolgt, der sich gut in den Ablauf der PLDA-Prozedur integrieren lässt. Ziel der Pilotstudie war es, die Anwendbarkeit dieser Einzelfaser-Spektroskopie-Methode zur Erfassung des mineralisationsgradabhängigen Streuverhaltens in Bandscheiben chondrodystropher Hunde zu untersuchen.

Material und Methoden: Die Pilotstudie wurde an insgesamt 21 Bandscheiben von 2 Hundeleichen („Hund A“ and „Hund B“) durchgeführt. Die Bandscheiben wurden zunächst mittels Computertomographie (CT), Radiographie und spektraler Rückstreumessung untersucht und anschließend histologisch evaluiert (Goldstandard). Die spektralen Rückstreumessungen (Spektralbereich: 500–950 nm) wurden mittels einer Einzelfaser durchgeführt, die über eine 20G Punktionsnadel im Gallertkern (Nucleus pulposus) der Bandscheiben positioniert wurde. Die Rückstreuspektren wurden einem Normalisationsalgorithmus unterzogen und in dimensionslose, wellenlängenabhängige Intensitäten umgewandelt. Die entsprechenden Intensitätsprofile wurden dann für den betrachteten Spektralbereich ausgewertet.

Ergebnisse: Insgesamt konnten durch die histologischen Untersuchungen 6 der 21 Bandscheiben als degeneriert identifiziert werden, 5 bei „Hund A“ und 1 bei „Hund B“. Mittels CT konnten ebenfalls alle 6 degenerierten Bandscheiben diagnostiziert werden. Mit der Radiographie wurden 2 der 5 betroffenen Bandscheiben bei „Hund A“ nicht erkannt. Die normierten Intensitätsprofile der 6 degenerierten Bandscheiben unterschieden sich deutlich von denen der anderen 15 „normalen“ bzw. schwach mineralisierten Bandscheiben. Die gemittelte Streuintensität der degenerierten Bandscheiben lag mit 2.79±0.58 (Mittelwert±SD) signifikant höher als bei den „normalen“ Bandscheiben, wo der Wert 1.48±0.37 betrug ($p<0.001$, Zwei-Stichproben t-Test).

Schlussfolgerung: Die durchgeführten Rückstreumessungen deuten darauf hin, dass der beobachtete Anstieg der Streuintensität mit dem Mineralisationsgrad der Bandscheibe assoziiert ist. Allerdings deckt der untersuchte Spektralbereich von 500–950 nm nicht die eigentliche Therapiewellenlänge der PLDA (2100 nm) ab, so dass die Veränderungen in den optischen Eigenschaften des Nucleus pulposus nicht direkt übertragbar sind. Weitere *In-vitro*- und *In-vivo*-Studien müssen sich anschließen, um die klinische Anwendbarkeit nachzuweisen.

Schlüsselwörter: Bandscheibendegeneration; Einzelfaser-Rückstreuungsspektroskopie; Streuung; Perkutane Laserablation der Bandscheibe.

1. Introduction

Acute or severe intervertebral disc herniation is a common, frequently debilitating, painful, sometimes fatal neurologic disease in the chondrodystrophic dog [1], and a similar condition of the intervertebral disc with extrusions or protrusions is also not uncommon in humans [2]. In dogs, this condition often occurs simultaneously along the entire vertebral column [3], and the most widely used prophylactic treatment for this disease in dogs is a highly invasive procedure known as surgical disc fenestration [4]. Although fenestration of canine intervertebral discs has been advocated, the benefits of this procedure remain controversial [5, 6], due to complications and a recurrence rate as high as 19.2% as reported by several large scale studies of a mixed population of dogs [7, 8].

Percutaneous laser disc ablation (PLDA), a minimally invasive procedure for intervention of intervertebral disc disease (IVDD) in human patients [9], was first adapted for the prevention of severe IVDD in dogs by one of the authors (Bartels) [10]. PLDA is performed by passing an optical fiber through a needle placed percutaneously in the center of a disc to introduce laser energy, most frequently from a 2100 nm holmium:YAG (Ho:YAG) laser. This laser surgical treatment photothermally ablates the disc material and fibrotic scar tissue forms which presumably prevents the disc from herniating and injuring the spinal cord in the future. A study on 277 cases revealed that prophylactic PLDA resulted in few complications and may reduce the risk of recurrence of signs of IVDD in dogs to as low as 3.4% [11].

Degeneration of the disc material is a precursor to intervertebral disc herniation [12]. The underlying etiology for most disc degeneration is associated with dehydration of the gelatinous nucleus pulposus, a metaplastic process that involves fibrotic metaplasia and deposition of a calcified mineral component within the nucleus [13]. This degenerative process is usually shown as opacification of the disc space on X-ray radiography [14], the current standard of diagnostic imaging for disc degeneration in dogs. Radiography is also used with PLDA surgery to guide the needle positioning into the center of each treated disc. However, radiography is not adequately sensitive in identifying the discs that should be treated, nor is it reliable for characterizing the degree of disc degeneration. When compared with histopathology, radiography has a sensitivity of 60% and specificity of 100% [15] of diagnosing disc degeneration. X-ray computed tomography (CT) and magnetic resonance imaging (MRI) have nearly 100% sensitivity in detecting disc degeneration and are useful in stratifying the degree of mineralization [16, 17]; however, due to the cost and inconvenience it is challenging to

standardize PLDA surgery under CT or MRI image guidance. Consequently, PLDA is performed on the most common sites of thoracolumbar IVDD, and with the same laser fluence applied to each thoracolumbar disc, regardless of its mineral content. Knowledge of individual disc mineral composition would allow treatment of degenerative discs that otherwise may have been missed, and permit laser energy dosage adjustments. An imaging/sensing technology that provides a more accurate pre-operative *in-situ* assessment of the disc mineralization, and potentially rapid post-operative feedback, could optimize the outcome of the PLDA procedure.

Visible and near-infrared (VIS/NIR) spectroscopy is an imaging technology widely used for noninvasive or minimally invasive sensing of tissue optical properties [18]. VIS/NIR spectroscopy relates the changes of the light spectra to the biochemical composition and micro-morphology of the tissue. Important tissue chromophores including oxygenated hemoglobin, deoxygenated hemoglobin, melanin, cytochrome oxidase, lipid, water, etc., have relatively strong and distinct VIS/NIR absorptions [19]. The structural assembly of sub-cellular organelle scatters VIS/NIR light with a signature wavelength-dependent pattern [20–22]. Quantification of the light spectra modulated collectively by absorption and scattering of tissue medium has thereby enabled VIS/NIR spectroscopy to assess tissue metabolic function and micro-architecture [23, 24]. Implementing VIS/NIR spectroscopy in needle-probing configuration is a natural choice for many demanding imaging applications. Needle-based VIS/NIR spectroscopy has been employed for staging of lung cancer through examination of mediastinal lymph nodes [25], for core-needle biopsy of breast cancer [26], for intra-operative differentiation of healthy and demyelinated peripheral nerves [27], etc. The current study investigates the feasibility of needle-based single-fiber VIS/NIR spectroscopy in sensing changes of optical scattering associated with mineral deposition in chondrodystrophoid canine intervertebral disc. The objective is to evaluate if needle-based single-fiber VIS/NIR spectroscopy could have higher accuracy of identifying degenerated intervertebral discs than the X-ray radiography does, and if needle-based single-fiber VIS/NIR spectroscopy could be rendered as a procedure compatible with PLDA work flow.

2. Materials and methods

This section justifies the configuration of single-fiber VIS/NIR spectroscopy in the context of rendering compatibility with PLDA procedure and accommodating the unique geometry that intervertebral disc morphology poses upon photon-sensing. It also describes the VIS/NIR spectroscopy system and the imaging protocol.

2.1. Single-fiber configuration for needle-based probing of intervertebral disc

The PLDA procedure employs a 20-gauge spinal needle (I.D. 495 μm), through which a 320 μm diameter low-OH fiber is inserted to deliver Ho:YAG laser irradiation (2100 nm) to ablate the nucleus pulposus. For an optical imaging modality to be compatible with the PLDA work flow, the delivery of the sensing fiber(s) has to utilize the same needle used for PLDA fiber introduction. To this end, there seem to be two ways to configure the imaging fiber: (1) a two-fiber configuration that illuminates and collects the light to and from the disc by different fibers; (2) a single-fiber configuration that illuminates and collects light through the same fiber. Whichever the configuration, the fiber being used for PLDA cannot be used simultaneously for the spectroscopy measurement, for the following reasons: (1) the tissue remission of the ablation level laser energy could easily destroy a photo-electronic detector used in such measurement, even though the detector could be insensitive to the ablation laser wavelength, unless a high-rejection filtering or time-multiplexing mechanism is implemented to prevent the PLDA light from reaching the photo-electronic detector through internal reflection or tissue remission; (2) the tip of the PLDA fiber deforms after laser firing, and is contaminated by the charcoal-like tissue remains caused by the ablation, which together alter the measurement consistency. To make the fiber configuration for spectroscopy stand-alone from the PLDA fiber implies a work flow of "insertion-retraction-insertion" for the sensing and PLDA, i.e., inserting measurement fiber(s) to evaluate the tissue, retracting the measurement fiber(s), and inserting PLDA fiber to ablate the disc that is evaluated as degenerated and therefore should be treated. By isolating the measurement fiber(s) from the PLDA fiber, one needs to choose between a two-fiber and a single-fiber configuration. The choice would now depend upon the mathematical or numerical model needed to quantify the photon collection, and whether or not the path of sensing light is to be impeded significantly by the neighboring anatomy of intervertebral disc.

The anatomic structure of an intervertebral disc [1] that could interfere with the photon path in needle-based fiber-sensing configuration is illustrated schematically in Figure 1. As is shown, the nucleus pulposus of the intervertebral disc is confined by an outer layer of annulus fibrosus and two neighboring vertebrae in the cranial and caudal aspects of the disc. The nucleus pulposus in the dog is approximately 5–15 mm in diameter and 1–2 mm in thickness, which to the photon propagation could form a "small-sandwiched-slab" geometry should the dimension of the geometry be comparable to the volume that photon propagates between the launching and collecting points. If running two fibers through this 20-gauge needle, the maximum lateral separation of the two fibers will be only 247 μm, a very small source-detector distance of which the characteristics of photon collection has not been adequately modeled by radiative transfer nor by Monte Carlo (MC) method [28]. Alternatively, two fibers could be placed and offset longitudinally with each other to produce a greater source-detector separation, with which the more convenient diffusion model could be used to quantify the photon remission. However, at source-detector separation of a few millimeters, photon remission may become nearly independent of the scattering parameters [29], and then the measurement will be sensitive to chromophore components [30] but insensitive to mineral deposition as the mineral deposition mostly affects the

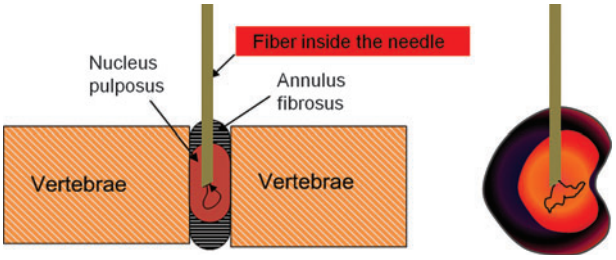

Figure 1 Schematic diagram of the sensing geometry that corresponds to probing the intervertebral disc with a fiber inserted into the nucleus pulposus through a needle placed for PLDA. The tip of the fiber is assumed to be custom-polished at an angle of 15°. Left panel: sagittal view when the subject in lateral recumbency; right panel: transverse view when the subject in lateral recumbency.

scattering of light. On the other hand, if the fibers are placed so the source-detector separation is greater than a few millimeters, the "banana-shape" light pass could easily be impeded by the vertebra, making the extraction of disc optical properties inaccurate and the measurement less sensitive to the scattering changes occurring in the nucleus pulposus. A single-fiber configuration is therefore the more attractive option for probing the optical properties of the intervertebral disc, when considering the modeling limitation imposed by the potentially "small-sandwiched-slab" sensing geometry and the prospect of using the same 20-gauge needle for PLDA.

2.2. Photon path length and sampling depth associated with single-fiber probing geometry

Single-fiber reflectance (SFR) spectroscopy of biological tissue collects light that has undergone either back reflection or a number of scattering events. The path of the light from leaving the fiber tip-face to returning to the same fiber tip is difficult to model analytically. Recently, Kanick et al. [31] applied MC modeling to study SFR spectroscopy in the spectral range of 550–800 nm. Using MC, they verified an empirical model for the photon path length $\langle L \rangle$ [32] and the sampling depth $\langle Z \rangle$ associated with single-fiber probing geometry, as follows

$$\langle L \rangle = \frac{1.34\, d_{fib}\, e^{0.17d}}{(\mu_s' \cdot d_{fib})^{0.23}(0.52+(\mu_a \cdot d_{fib})^{0.52}} \quad (1)$$

$$\langle Z \rangle = \frac{0.38\, e^{-0.06\mu_a \cdot d_{fib}}}{(\mu_s' \cdot d_{fib})^{0.12}} \langle L \rangle \quad (2)$$

Where d_{fib} is the diameter of the fiber in the unit of mm, μ_a is the absorption coefficient in the unit of mm^{-1}, and μ_s' is the reduced scattering coefficient in the unit of mm^{-1}, therefore $\mu_s' \cdot d_{fib}$ and $\mu_a \cdot d_{fib}$ are two dimensionless terms. Note that the path length and sampling depth are values averaged over the ensemble of photon trajectories. This specific empirical model was deduced in [31] and [32] for the range of parameters including μ_a=0.1–3 mm^{-1}, μ_s' =0.2–4 mm^{-1}, and d_{fib}=0.2–2 mm. It is of note that although the studies of [31] and [32] were specific to semi-infinite media, the empirical models that formulate the dominance of scattering events proximal to the fiber tip in single-fiber configuration are shown to be applicable to the measurement made in virtually an infinite medium by submerging the fiber-probe tip a few millimeters into intralipid phantom [33]. The insensitivity of the SFR measurement to medium boundary geometry is comprehensible as photons hitting the boundary at positions away from the single fiber are very unlikely to be eventually collected by the single fiber of a limited numerical aperture.

This study applied the empirical model given in Eqn. (1) and (2) to evaluating how likely the probing light would interfere with the vertebrae and annulus fibrosus. For this study the parameters in Eqn. (1) and (2) are evaluated at broad ranges of μ_a=0.001–1 mm^{-1} and μ_s' =0.1–10 mm^{-1}, for a fixed fiber diameter of d_{fib}=0.32 mm as routinely used in PLDA. The estimated photon path length and sampling depth are shown in Figure 2. The salient feature observed from Figure 2 is that the path length and the sampling depth are much more affected by the reduced scattering than by the absorption characteristics, and the stronger the reduced scattering is, the smaller the path length and sampling depth are. The shaded area corresponds to a sampling depth <0.75 mm and a photon path length <1.5 mm. The shaded area is also associated with a range of μ_a=0.001–0.1 mm^{-1} and μ_s' =0.3–10 mm^{-1}, both being much broader than optical properties associated with typical scattering-dominant biological tissue. It will be shown later that the μ_s' of the nucleus pulposus extracted from the measurement appears to be greater than the maximum μ_s' evaluated in Figure 2, thus for a fiber placed in the middle of the nucleus pulposus, the photon path length and sampling depth would be considered <0.7 mm and 0.3 mm, respectively. Any interference from the annulus fibrosus and neighboring vertebra to the single-fiber sensing at the center of the nucleus pulposus is thus expected to be negligible.

2.3. Single-fiber VIS/NIR spectroscopy system for probing intervertebral disc

Based on the previous justification regarding the feasibility of probing the nucleus pulposus of intervertebral disc in a "small-sandwiched-slab" sensing geometry, a single-fiber VIS/NIR reflectance spectroscopy system was constructed. The system is shown schematically in Figure 3. The light source contained a compact deuterium tungsten source module (L10671; Hamamatsu Photonics, Japan) and a 940 nm light-emitting diode (LED) (M940L2; Thorlabs, Newton, NJ, USA). The 940 nm LED source was originally implemented to enhance the measurement sensitivity to the light absorption by water content, and kept in the system even though later it was found that the effect of water absorption to the remission spectrum was significantly less remarkable than the scattering.

Each of the two light source modules was coupled to one branch (200 µm diameter fiber) of a bifurcated fiber bundle "A" (BIF200-VIS/NIR; Ocean Optics Inc., Dunedin, FL, USA) that integrated the spectra of the two light sources at the combining branch. The combining branch of the fiber bundle "A" was coupled to one branch (400 µm diameter fiber)

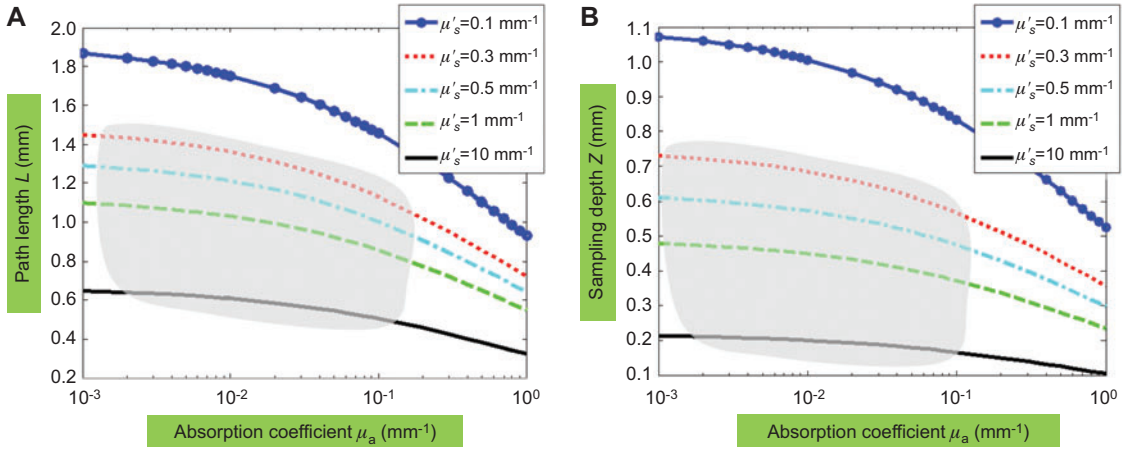

Figure 2 Photon path length and sampling depth evaluated for single-fiber probing geometry based on the empirical model in [31, 32]. (A) Path length and (B) sampling depth. The μ_a and μ'_s are evaluated over a range of 3-orders and 2-orders, respectively. The shaded area corresponds to the estimate of the path length and sampling depth for typical biological tissue.

of a second bifurcated fiber bundle "B" (BIF400-VIS/NIR; Ocean Optics Inc., Dunedin, FL, USA), the other branch of which was connected to a compact spectrometer (NT58-303; Edmund Optics Inc., Barrington, NJ, USA) with a working range of 350–1050 nm. The combining branch of the fiber bundle "B" was connected to a standard PLDA low-OH fiber of 320 µm in diameter (H320R; New Star Lasers Inc., Roseville, CA, USA). This fiber was placed in the tissue by inserting it through a 20-gauge spinal needle routinely used in PLDA procedure. The tip of the PLDA fiber was custom-polished to an angle of 15°. This angle-polishing helped to reduce the back reflection of the light at the tip [25]; however, there was still reflection at the fiber tip and at other intermediate connecting facets of the fiber channels. The native spectrum collected by placing the fiber in the air is shown in Figure 3 as the up-right inset, which showed an effective system-spectral range of approximately 500–950 nm, with numerous spikes due to coupling of ambient illuminations. These spike noises were smoothed out by filtering.

2.4. Study protocol

The study protocol on live animals was approved by the Institutional Animal Care and Use Committee of Oklahoma State University. However, as this pilot study aimed to examine whether the SFR spectrum can be used to differentiate a degenerative disc from a normal disc, the study was performed on two cadaveric dogs only ("Dog A" and "Dog B"). Diagnostic imaging of the intervertebral discs of the cadaveric dogs was performed by radiography and CT. Right lateral

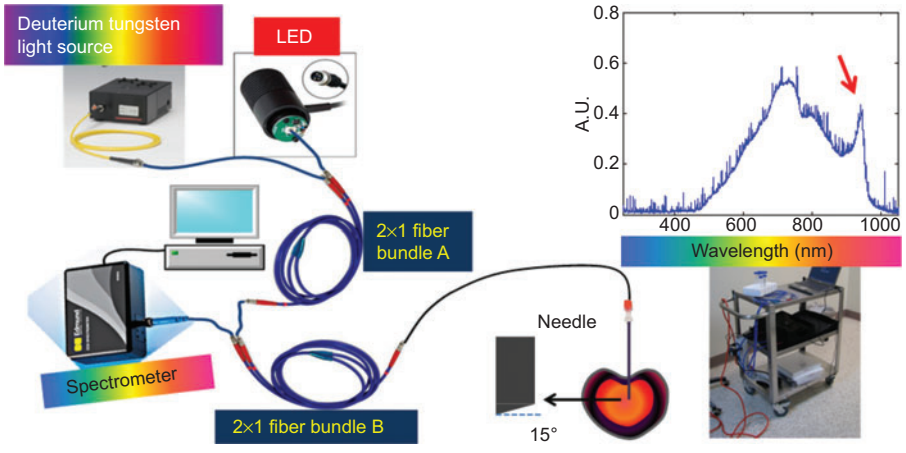

Figure 3 Configuration of the SFR spectroscopy system. A compact deuterium tungsten source module and a 940 nm LED were coupled by a bifurcated fiber bundle "A" to one branch of a second bifurcated fiber bundle "B" whose other end was connected to a compact spectrometer. The combining branch of the fiber bundle "B" was connected to a standard PLDA fiber for placing into the tissue through a spinal needle. The tip of this fiber was custom-polished to an angle of 15°. The up-right inset shows the background spectra due to internal reflection. The lower right inset is the photograph of the system placed on a small stainless steel cart for operating room use.

radiographs were obtained along the entire thoracolumbar spine as an initial screening modality for mineralized intervertebral discs. Images were acquired using digital radiography (Eklin Medical Systems Inc., Santa Clara, CA, USA). CT of the spines was performed using a 4-slice CT scanner (GE Lightspeed Plus; General Electric Healthcare, Milwaukee, WI, USA). Dogs were scanned in dorsal recumbency from the 8th thoracic to the 6th lumbar vertebra. Dogs were scanned using helical acquisition with the following parameters: 175 mA, 120 KVp, 0.625 mm slice thickness, 0.625 mm interval, and differing gantry tilts for each disc space to ensure images acquired were parallel with the intervertebral disc. Reconstructions were performed with 0.625 mm thickness and intervals. Images were reviewed by one of the authors (McKeirnan), a senior surgical resident with guidance from a board-certified radiologist if questions arose.

After radiographic and CT imaging, the dogs were placed in lateral recumbency and a 20-gauge needle passed through the epaxial musculature into the center of each intervertebral disc space using a technique previously described for PLDA [10]. Needles were placed into the discs from T (denoting "thoracic") 8–9 to L (denoting "lumbar") 5–6, including T10–11 to L4–5 which are considered the most common sites of intervertebral disc degeneration, as well as surrounding sites where needles could be successfully placed for additional data collection. Anatomical variants prevented the placement of needles in T8–9 in "Dog B". After the position of the needle had been verified by biplane fluoroscopy, the stylet of the needle was retracted and the imaging fiber was passed through the needle, as shown in Figure 4. To prevent the needle tip from interrupting the sensing light, the sensing fiber was positioned approximately 1 mm distal to the needle tip by a marker placed on the proximal end of the fiber. For each disc, five repeated spectral measurements were taken at a total integration time of 10 s (2 s per measurement). The acquisition time scale was limited by the weak illumination of the compact tungsten light source. The acquired spectra data were processed off-line using the method introduced in the later sections of this paper. After completing the measurements, 40–60 s of PLDA was performed on selected discs using a 2W Ho:YAG laser. Single-fiber spectroscopy measurements were also acquired from the discs after PLDA procedure.

2.5. Histopathology

After the spectral measurements and PLDA, the vertebral columns were isolated and intervertebral discs were harvested with 2–3 mm sections of vertebral end plate left on either side using a bench top band saw. Each vertebral disc unit was labeled and fixed in 10% buffered formalin for 5–7 days. Transverse sections through the center of each disc were then collected using a scalpel and placed in a cartridge and further fixed in fresh 10% buffered formalin prior to processing for histopathological examination. Transverse sections of tissue from the ablated areas were dehydrated in serial alcohol dilutions, cleared in toluene, and embedded in paraffin. Embedded tissues were sectioned on a microtome and 6–10 μm thick sections were mounted on glass slides, deparaffinized, rehydrated and stained with hematoxylin and eosin, as well as the von Kossa stain to quantify mineralization, and then examined under a light microscope. The original mineralization in the nucleus pulposus was estimated based on the amount of mineral present in histopathological sections compared to the amount of intact nucleus available for evaluation.

3. System calibration

This section analyzes a spectral normalization method used to extract the wavelength-dependent scattering intensity profile from the raw remission spectra. The method was tested with liquid tissue phantom of controlled scattering properties.

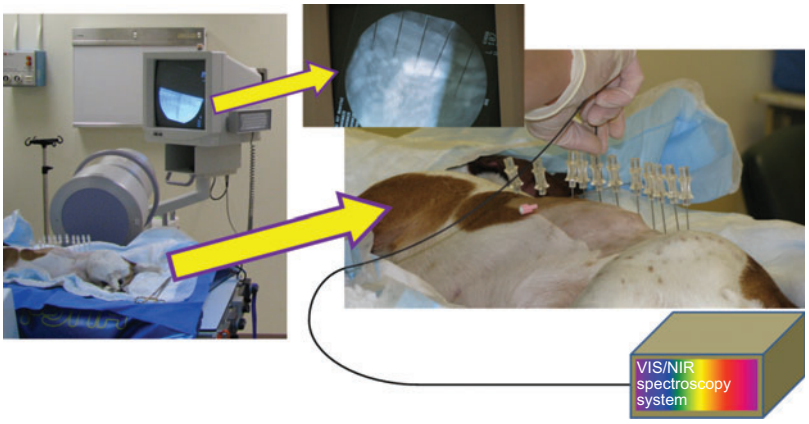

Figure 4 The procedure for SFR spectroscopy of nucleus pulposus. A 20-gauge needle was passed through the posterolateral position in the thoracolumbar disc spaces of the animals under biplane fluoroscopy, as shown in the left panel. After retracting the stylet of the needle, the imaging fiber was passed through the needle and positioned approximately 1 mm distal to the tip of the spinal needle by a marker placed on the proximal end of the fiber. After completion of the spectroscopy measurements on all the discs, PLDA was performed by using a different fiber. Spectroscopy measurements were also performed on each disc following the PLDA procedure.

3.1. Normalization of the wavelength-dependent scattering spectrum

The baseline spectral profile from the light source had significant intensity variation over its spectral range, as that shown in Figure 3. The mineralization in the intervertebral disc was expected to increase the light scattering; however, the overall intensity of the remission spectrum could be affected by both the scattering and absorption properties of the sampled medium. The intervertebral disc is nearly avascular [13], which renders an additional benefit as the sensing measurement is not affected by the strong absorption of hemoglobin as seen in many other biological sensing applications. Biological tissue, however, is known to exhibit a scattering characteristic in the VIS/NIR band as that the scattering usually reduces as the wavelength increases. To quantify the effect of the mineral deposition to the spectral remission from intervertebral disc, it is necessary to deduce from the remission spectrum the wavelength-dependent scattering characteristics. The method used in this study to extract the wavelength-dependent scattering characteristics of the sampled medium was based upon an approach practiced in [25] but with slight modifications.

Consider $S(\lambda)$ as the system-level native spectral profile of delivering light to and collecting from the sampling medium through a single-fiber configuration. When the VIS/NIR light is incident upon air or water that has negligible backscattering, as illustrated in Figure 5A, the reflectance spectra $R(\lambda)$ can be modeled by

$$R_{air}(\lambda)=\eta_c\cdot\eta_{fib/air}S(\lambda)+\eta_{\text{int}}S(\lambda) \tag{3}$$

for air and

$$R_{wat}(\lambda)=\eta_c\cdot\eta_{fib/wat}S(\lambda)+\eta_{\text{int}}S(\lambda) \tag{4}$$

for water, respectively, where η_c is the collection efficiency of the fiber [32] approximated as a constant in this study, $\eta_{fib/X}$ represents the Fresnel reflection at the fiber/medium interface, and η_{int} denotes the combined effect of all internal reflections within the fiber paths. When the fiber is placed in a scattering medium as is shown in Figure 5B, the remission contains the scattered light and this could be modeled [33] as

$$R_{med}(\lambda)=\eta_c \left\{\frac{\left[\mu_S'(\lambda)\cdot d_{fib}\right]^{\rho_2}}{\rho_1+\left[\mu_S'(\lambda)\cdot d_{fib}\right]^{\rho_2}}\exp\left[-\mu_a(\lambda)\cdot\langle L\rangle\right]S(\lambda)+\eta_{fib/med}S(\lambda)\right\} +\eta_{\text{int}}S(\lambda) \tag{5}$$

where $\mu_s'(\lambda)\cdot d_{fib}$ is a dimensionless term as that given in Eqn. (1) and (2). The fraction term containing $\mu_s'(\lambda)\cdot d_{fib}$ implies that for a fixed fiber diameter, as is true in a given system, the remission intensity is nearly linear to $\left[\mu_s'(\lambda)\right]^{\rho_2}$ in a weak scattering medium, and levels off and thereby becomes independent upon $\left[\mu_s'(\lambda)\right]^{\rho_2}$ in a very strong scattering medium. We then normalize the reflectance spectrum from the scattering medium with respect to the reflectance spectra from water and air by

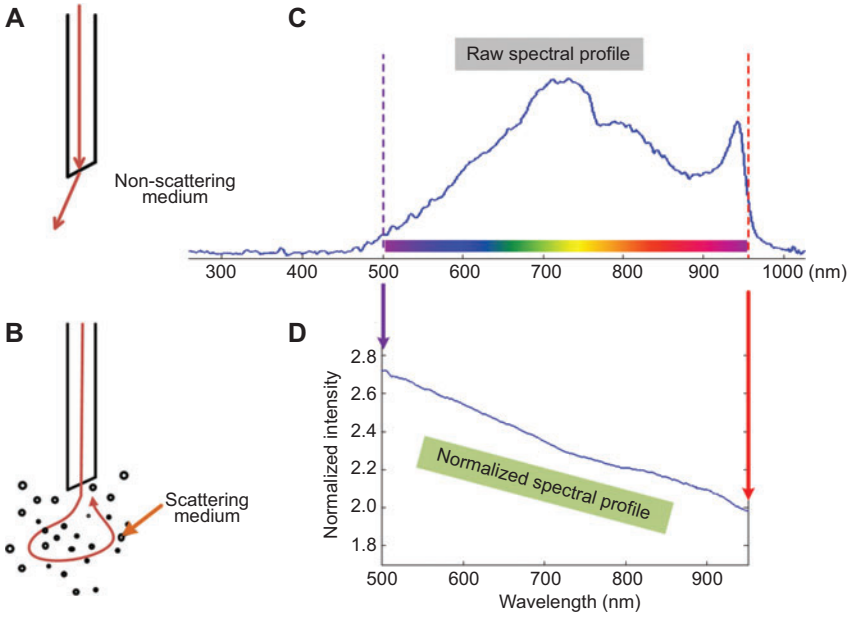

Figure 5 Normalization methods. (A) In non-scattering medium, the fiber collects specular reflection. (B) In scattering medium, the fiber collects back-scattered light in addition to the specular reflection. (C) A raw spectra profile obtained from 10% intralipid solution and after smoothing by a Savitzky-Golay filter. (D) Normalized spectral profile of the one in (C) in the range of 500–950 nm with respect to the spectra from water and air by use of the formula given in Eqn. (6).

$$R_{norm}(\lambda)=\frac{R_{med}(\lambda)-R_{wat}(\lambda)}{R_{air}(\lambda)-R_{wat}(\lambda)} \tag{6}$$

then it comes to

$$R_{norm}(\lambda)=\frac{\left[\mu_S'(\lambda)\cdot d_{fib}\right]^{\rho_2}}{\rho_1+\left[\mu_S'(\lambda)\cdot d_{fib}\right]^{\rho_2}}\exp\left[-\mu_a(\lambda)\langle L\rangle\right]+\left[\eta_{fib/med}-\eta_{fib/wat}\right]\Big/\left[\eta_{fib/air}-\eta_{fib/wat}\right] \tag{7}$$

Since the refractive index of the tissue is very close to that of water, $[\eta_{fib/med}-\eta_{fib/wat}]$ could be neglected, and by denoting $[\eta_{fib/air}-\eta_{fib/wat}]$ as $1/\xi$, Eqn. (7) changes to

$$R_{norm}(\lambda)\approx\xi\frac{\left[\mu_s'(\lambda)\cdot d_{fib}\right]^{\rho_2}}{\rho_1+\left[\mu_s'(\lambda)\cdot d_{fib}\right]^{\rho_2}}\exp\left[-\mu_a(\lambda)\langle L\rangle\right] \tag{8}$$

The outcome of the spectral normalization expressed by Eqn. (6) is presented in Figure 5C,D. Figure 5C represents a raw remission spectrum obtained from 10% intralipid solution, after applying a Savitzky-Golay filter to suppress any spike noise as that shown in the inset of Figure 3 and a moving average over 100 pixel points to further smooth the spectrum. The measurement of the air and water were performed in "dark conditions" to minimize the effect of ambient lighting. Implementing Eqn. (6) to the spectrum in Figure 5C over the effective source band of 500–950 nm leads to the spectrum in Figure 5D. For intralipid, water is the main absorber and the $\mu_a(\lambda)$ in the 500–950 nm range for intralipid is of the order of 0.002–0.003 mm^{-1}. Therefore, the exponential term in Eqn. (8) is nearly 1 over 500–950 nm range for sub-millimeter path lengths. The normalized spectral profile $R_{norm}(\lambda)$ should then demonstrate a characteristic which is mainly dependent on $\left[\mu_s'(\lambda)\right]^{\rho_2}$, i.e., the reduced scattering coefficient. The decreasing trend of the normalized spectral intensity with increasing wavelength as shown in Figure 5D agrees with the wavelength-dependent power-law characteristics of $\mu_s'(\lambda)=A\lambda^{-b}$ and, subsequently $\left[\mu_s'(\lambda)\right]^{\rho}=A^{\rho}\lambda^{-b\rho}$, where A is the scattering amplitude and b is the scattering power.

3.2. Single-fiber VIS/NIR spectroscopy of intralipid phantom of varying concentration

The ability of relating the remission intensity with the scattering properties of the medium as represented by Eqn. (6) was further tested for intralipid solution of varying concentrations. The results are shown in Figure 6A, for the concentration of intralipid including 0.5%, 1–6%, 8%, 10%, 12%, 14%, 16%, 18% and 20%. Six rounds of tests were made for each concentration of the intralipid. The normalized spectra clearly showed that scattering intensity increased as the concentration of intralipid increased. The normalized scattering intensity in a 4.3 nm range around 632.8 nm (red dashed line) were extracted from Figure 6A, and plotted in Figure 6B against the known values of $\mu_s'\approx127.0\,[c]-205.3\,[c]^2$, where $[c]$ is the concentration of intralipid [34]. A fitting to the measurement data by use of Eqn. (8), when neglecting the exponential term accounting for absorption, leads to the following result

$$R_{norm}(\lambda_0)\approx8.0587\frac{\left[\mu_s'(\lambda_0)\cdot0.32\right]^{1.1586}}{9.6974+\left[\mu_s'(\lambda_0)\cdot0.32\right]^{1.1586}} \tag{9}$$

with a Pearson correlation coefficient of r=0.9999. Of the fitted values in Eqn. (9), ρ_1=9.6974 and ρ_2=1.1586, which are comparable to the range [9.014–8.389] and [1.090–1.054] estimated for ρ_1 and ρ_2, respectively, in 650 nm by a MC study [33]. Note that the value of ξ=8.0587 indicates a 12.4% higher specular reflection from the fiber/air interface than from the fiber/water interface.

4. Results

This section reports the outcome of VIS/NIR spectroscopy of a total of 21 discs from two cadaveric dogs compared

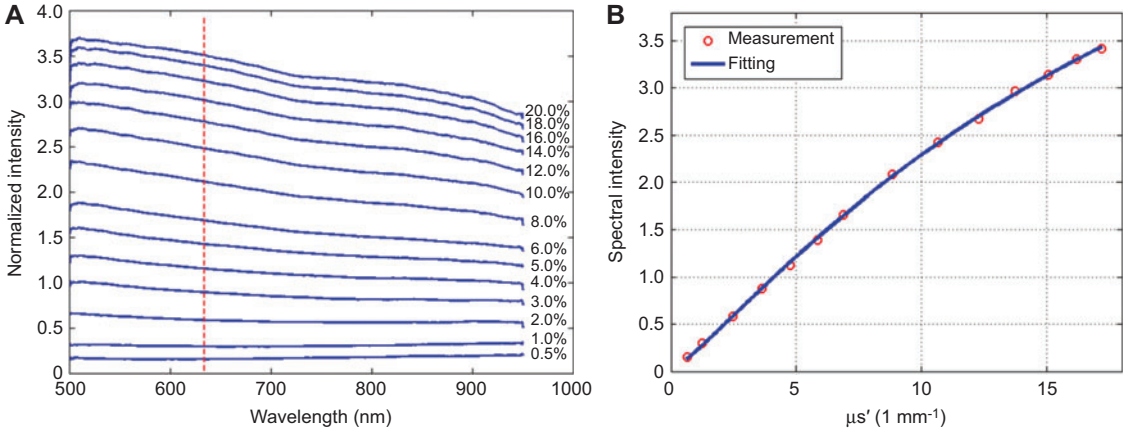

Figure 6 Normalization with various levels of reduced scattering using intralipid. (A) Normalized spectral profiles associated with intralipid concentrations of 0.5–20%. The mean spectral intensity in a 4.3 nm range around 632.8 nm as indicated by the red line is plotted vs. calculated reduced scattering coefficient in (B). The fitting is based on Eqn. (8) without considering the absorption term.

to X-ray radiography and CT, and histopathology results. The single-fiber VIS/NIR spectroscopy has found that the six degenerated discs had substantially higher scattering intensities than the 15 normal or insignificantly mineralized discs.

4.1. Radiography and X-ray CT

Radiographic and CT imaging were performed on all thoracic and lumbar intervertebral discs of the two cadaveric dogs. The needles for VIS/NIR sensing and subsequently for PLDA were placed successfully in "Dog A" from T8–9 to L5–6 and in "Dog B" from T9–10 to L5–6. Therefore only the radiography and CT images of those discs being evaluated by VIS/NIR measurement are displayed in Figure 7. Of "Dog A", T10–11, T11–12, and L3–4 were shown mineralized on radiography. CT scan detected mineralization of T10–11, T11–12, and L3–4, while revealing small amounts of mineral within T8–9, T9–10, and conspicuous composition in T12–13. In "Dog B", only T11–12 was shown by radiography to be mineralized, and the CT scan confirmed that only T11–12 was mineralized.

4.2. Histopathological results

Histopathology confirmed mineralization within the nucleus pulposus of T8–9, T9–10, T10–11, T11–12, and L3–4 in "Dog A" and T11–12 in "Dog B", based on intensely positive von Kossa staining in these samples. In "Dog A", approximately 35% of the examined nucleus of T8–9, 15% of T9–10, 20% of T10–11, 80% of T11–12, and 100% of L3–4 was mineralized. In "Dog B" approximately 70% of the examined nucleus of T11–12 was mineralized. Additional areas of mineralization in T12–13 of "Dog A" appeared to be artifactual sections of bone from the vertebral endplate, a complication of disc processing techniques and collapse of the disc space from a previous surgery. Small focal areas of mineral were found in the nucleus of T13–L1 and L1–2 of "Dog A", and T9–10, T10–11, and L5–6 of "Dog B" representing <3–5% of the examined nucleus in these samples.

4.3. Single-fiber VIS/NIR spectroscopy

The normalized VIS/NIR spectroscopy measurement of those 11 intervertebral discs of "Dog A" and 10 intervertebral discs of "Dog B" are given in Figure 8A,B. The dashed curves were from T8–9, T9–10, T10–11, T11–12, L3–4 of "Dog A", and T11–12 of "Dog B", the six intervertebral discs identified by the CT and confirmed by histopathology as being mineralized. The solid curves were from the rest of the 15 intervertebral discs identified by the CT and confirmed by histology as not having a detectable level of mineralization. For each dog, the normalized spectral intensities corresponding to the mineralized discs are consistently higher than those corresponding to the discs of

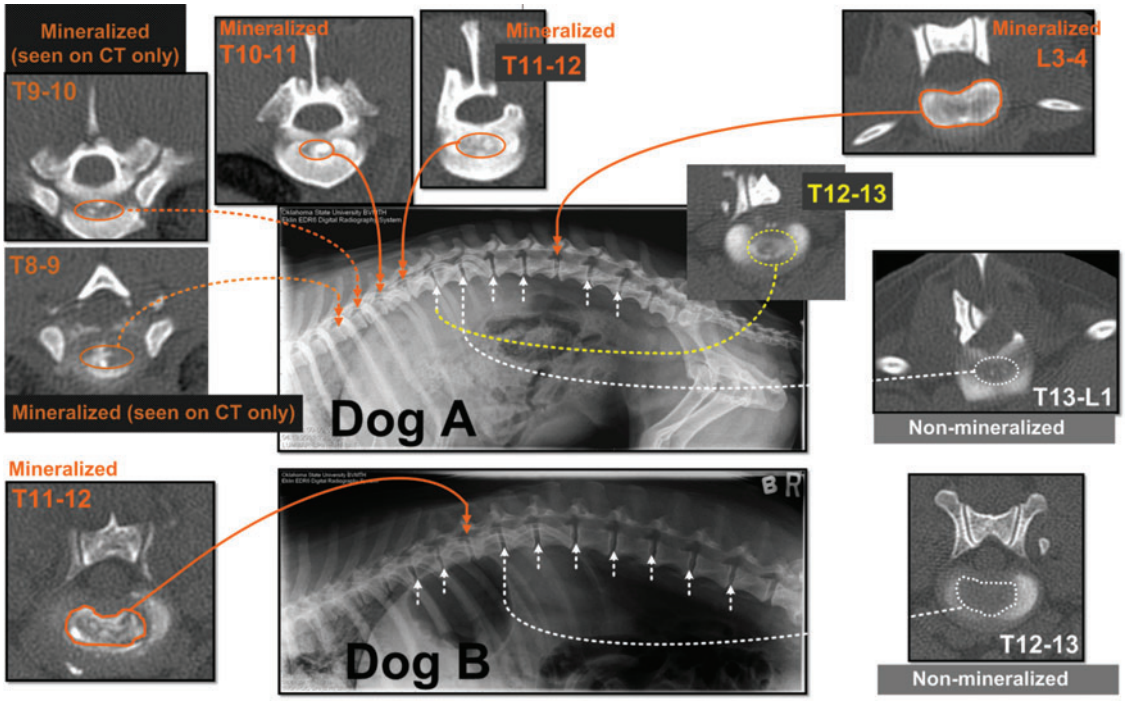

Figure 7 X-ray radiography and CT imaging of the intervertebral discs of "Dog A" and "Dog B". Upper panel for "Dog A": on digital radiography, T10–11, T11–12, and L3–4 were mineralized. T10–11, T11–12, and L3–4 were confirmed (indicated by solid line with double arrow) as mineralized by CT, which also discovered additional degenerated discs T8–9, T9–10 (indicated by dashed line with double arrow) and conspicuous composition in disc T12–13. Lower panel for "Dog B": on digital radiography, only T11–12 was mineralized. CT confirmed the radiographic finding. The nucleus pulposus of the six degenerated discs are outlined by the solid curve, and the nucleus pulposus of one normal disc T13–L1 of "Dog A" and one normal disc T12–13 of "Dog B" are outlined by the dashed curve.

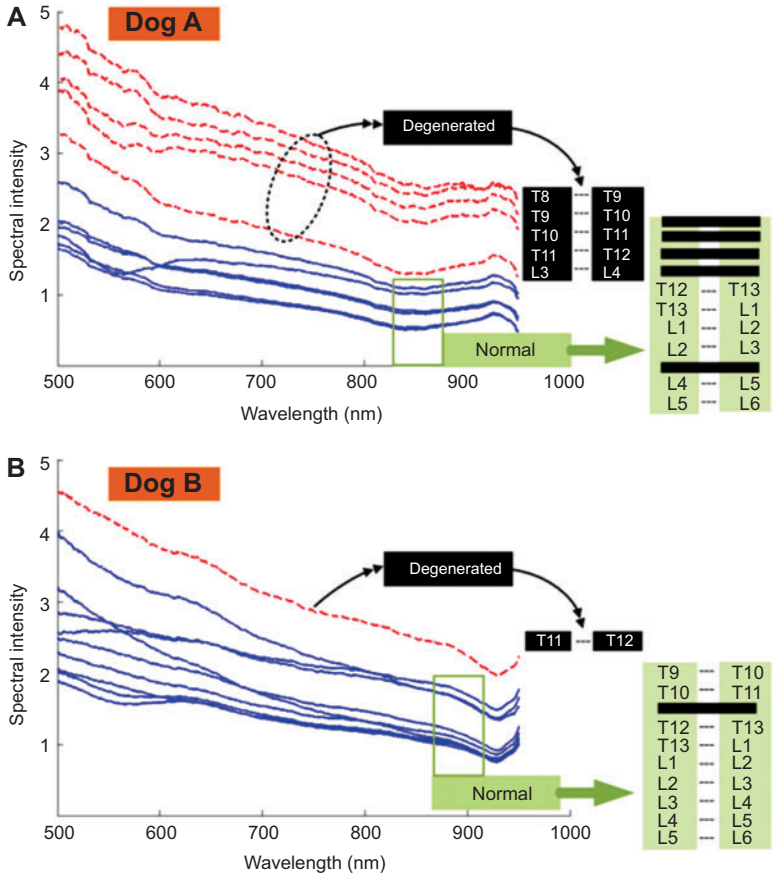

Figure 8 Normalized spectra of the intervertebral discs of "Dog A" and "Dog B". The black bars in the legend mark T8–9, T9–10, T10–11, T11–12, and L3–4 of "Dog A" and T11–12 of "Dog B" that are indicated by CT as degenerated. The spectra of these discs are plotted as the dashed curves. The spectra of the rest of the normal or insignificantly mineralized discs are plotted as the solid blue curves.

no or insignificant mineralization. The spectral intensity values of mineralized or normal discs, however, have shown inter-subject variations. If the intensity curve is averaged over the entire spectral range from 500 to 950 nm for the discs of both "Dog A" and "Dog B", the six degenerated discs have a mean spectral intensity of 2.79 with a standard deviation of 0.58, and the 15 normal or insignificantly mineralized discs have a mean spectral intensity of 1.48 with a standard deviation of 0.37, as summarized in Figure 9. The average spectral-wide intensity of the mineralized discs is nearly two-folds of that of the normal or insignificantly mineralized discs, with broader standard deviation. A statistical power of $p<0.001$ is found for the difference between the spectral intensities of the mineralized and normal or insignificantly mineralized discs, after applying a two-sample *t*-test to the two small-size samples.

5. Discussion

This study has been based on the hypothesis that the mineral deposition in intervertebral disc increases the scattering of light in the VIS/NIR range. Although the measurements were limited to 21 intervertebral discs of only two cadaveric dogs, the six degenerated discs revealed noticeably stronger VIS/NIR scattering than the normal discs did, with appreciable inter-subject variations. It is interesting to compare the average scattering spectra of the normal and degenerated

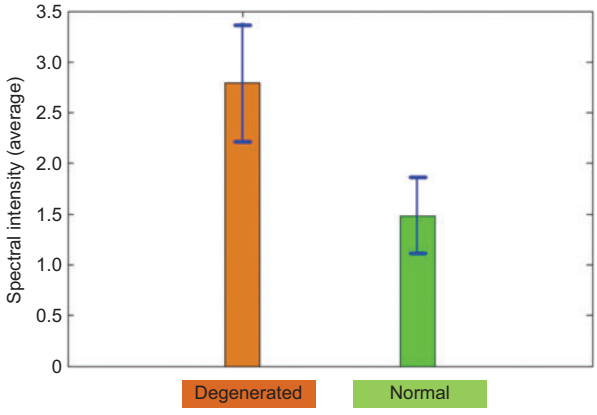

Figure 9 The intensity averaged over the range of 500–950 nm for each of the spectral profiles shown in Figure 8. The group of degenerated discs has a sample size of six, and intensity mean of 2.79 with a standard deviation of 0.58. The group of normal discs has a sample size of 15, and intensity mean of 1.48 with a standard deviation of 0.37 ($p<0.001$).

intervertebral discs with the spectrum of intralipid phantom at different concentrations, as shown in Figure 10, where the spectrum of intervertebral disc was averaged for the group that was either normal or degenerated from both dogs. Within the shown 500–950 nm range, the scattering profile of the 15 normal or insignificantly mineralized discs seems to lie between that of 4 and 8% intralipid; whereas the scattering profile of the six degenerated discs seems to be stronger than that of 10% intralipid at longer wavelength range and even stronger than 20% intralipid at shorter wavelength range. There is a salient difference in the slope of the spectral profile between normal or degenerated disc and intralipid. It is well-known that biological tissue reveals a power-law wavelength-dependent reduced scattering characteristics as represented by $\mu_s'(\lambda)=A\lambda^{-b}$. The scattering amplitude A is proportional to the number density of the scattering particles; whereas the scattering power b is determined by a number of factors including the average size of the scattering particle, the size distribution of the scattering particle [35], etc. The much steeper declining of the spectral intensity of the intervertebral disc with wavelength increase, whether the intervertebral disc is degenerated or not, indicates that the microscopic compositions in the nucleus pulposus has a higher scattering power than does the lipid droplets in intralipid solution. The effects of scattering particle size and size distribution on the scattering power are interplayed, yet the scattering size appears to have dominant effect on the scattering power for average scatter size smaller than 200 nm [35]. The size distribution of the scattering particles in 10% intralipid was determined by transmission electron microscopy to be exponential, with an average particle size of 97±3 nm [36]. It is then speculated that the scattering particles in the nucleus pulposus are at sub-100 nm range on average, should they follow an exponential size distribution.

To extract the scattering amplitude and scattering power information from the spectral profile, however, needs the absorption contribution to the measured spectral remission

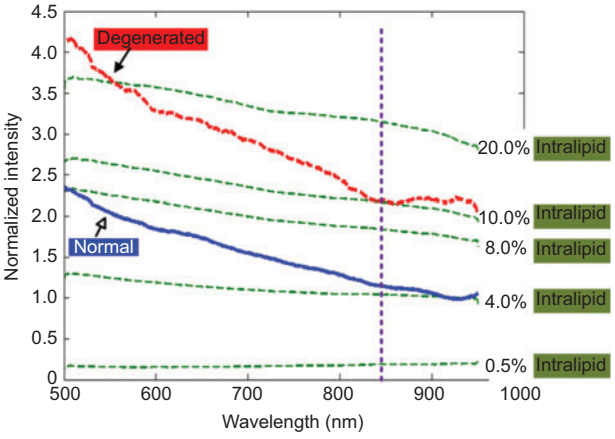

Figure 10 Normalized spectral profiles of normal or insignificantly mineralized (solid–blue) and degenerated (dashed–red) intervertebral discs vs. the spectral profile of intralipid of different concentrations (lighter dashed–green).

to be accounted for. In the shorter wavelength range of the 500–950 nm band the spectral profile is not as smooth as that of the intralipid; however, it is not to be altered significantly by the hemoglobin absorption spectrum owing to the avascularity of the intervertebral disc. In the longer wavelength range of the 500–950 nm band, the spectral profile of intervertebral disc is much more varying than that of the intralipid, specifically for the ones measured from degenerated discs. A close-up inspection of the spectral profile of the intralipid solutions showed a decreasing trend from 850 toward 950 nm, and conversely, the spectral profile of the intervertebral disc showed an increasing trend from 850 toward 950 nm. The normal intervertebral disc is expected to be nearly absent of lipid and is lower in water concentration as compared to intralipid. The slight up-bending of the spectral profile of normal intervertebral disc above 850 nm, compared to that of intralipid, corresponds to the lower attenuation near the lipid and water absorption peak around 950–1000 nm. The degeneration of the intervertebral discs is known to be accompanied by dehydration. The more upward bending of the spectral profile of degenerated intervertebral disc above 850 nm, compared to that of normal disc, should indicate loss of water content in the water absorption peaks around 950–1000 nm. Should the source-spectrometer assembly used in this system have sufficient spectral sensitivity above 1000 nm, the changes in intervertebral disc due to the change in water concentration might have been better revealed.

This study is limited in its sensitivity to mineralization occurring in the periphery of the nucleus pulposus, due to the placement of the fiber in the center of the nucleus pulposus and the limited sampling volume of the VIS/NIR spectroscopy measurement. Further study may be necessary to compare the VIS/NIR spectral intensity from one intervertebral disc with the Hounsfield units [37] averaged over the same disc, to examine if there is correlation between VIS/NIR spectral intensity with the volume ratio of the mineralization to the nucleus pulposus. Should the VIS/NIR spectral intensity discriminate the degree of mineralization in the nucleus pulposus, it may be used as an effective evaluation tool to adjust the fluence of PLDA according to the grade of disc degeneration, by developing an in-line data processing routine with more user-friendly control and calibration features. The scattering characteristics of the nucleus pulposus measured over a spectral range of 500–950 nm in this study may not necessarily represent the optical properties of the nucleus pulposus at the laser wavelength used for PLDA (2100 nm); however, a more concrete determination of the onset and potentially the degree of disc degeneration will provide an objective measure to perform the PLDA and to adjust the fluence. An earlier study [38] evaluated the rate of absorption and scattering optical properties of degenerative disc material in the range of 200–2200 nm in 16 post-mortem discs using a spectrophotometric unit. High rates of diffuse remittance were found for NIR laser wavelengths, indicating only low rates of absorption which substantiates this current study. In contrast, much higher rates of absorption were determined for mid-infrared lasers which are more appropriate for laser discectomy. If the SFR spectroscopy is to be performed in a spectral range covering

mid-infrared as with the Ho:YAG laser for PLDA, the measurements could indicate more directly the optical properties of the disc in the treatment spectrum, but the strong absorption has to be de-coupled from the measurement spectra to characterize the scattering changes associated with mineralization. As the mineralization is associated with change of collagen content in the nucleus pulposus, laser-induced fluorescence [39] may be considered as an alternative method for detecting the disc degeneration.

6. Conclusion

Needle-probing SFR spectroscopy has been used to measure the scattering associated with mineralization in canine intervertebral discs over a spectral range of 500–950 nm.

A pilot study was performed on a total of 21 intervertebral discs belonging to two cadaveric dogs. The discs were imaged by radiography, then SFR spectroscopy, and CT before carrying out histopathologic examination. CT diagnosed six out of 21 degenerated discs, with a conspicuous finding of one more disc that was shown by histopathology as a false-positive, whereas radiography missed two of the five degenerated discs of one dog. There was a noticeable difference of the averaged scattering intensity between the group of degenerated disc (2.79±0.58) and the group of normal or insignificantly mineralized disc (1.48±0.37) with a statistical power of $p<0.001$ based on a two-sample *t*-test performed on the small-size study. Although needle-probing SFR spectroscopy has shown that the increase in light scattering intensity across the entire 500–950 nm spectral range is associated with the mineralization in canine intervertebral discs, studies on more cadaveric and eventually *in-vivo* samples are necessary before the clinical feasibility can be established. Furthermore it is of note that the scattering characteristics of the nucleus pulposus measured in this study may not necessarily represent the optical properties of the nucleus pulposus at the laser wavelength used for PLDA.

Acknowledgements

This work has been supported in part by an endowment fund from Kerr Foundation, Oklahoma City, and a research grant HR11–0043 from Oklahoma Center for the Advancement of Science and Technology (OCAST). The authors acknowledge Dr. Robert Bahr, DACVR, Carolyn Rodebush, John Horne, and Sue Mott for their assistance in obtaining and interpreting the diagnostic images used in this study.

References

[1] Bray JP, Burbidge HM. The canine intervertebral disk: part one: structure and function. J Am Anim Hosp Assoc 1998;34(1):55–63.

[2] Johansen JP, Fossgreen J, Hansen HH. Bone scanning in lumbar disc herniation. Acta Orthop Scand 1980;51(4):617–20.

[3] Olsson SE, Hansen HJ. Cervical disc protrusions in the dog. J Am Vet Med Assoc 1952;121(908):361–70.

[4] Yturraspe DJ, Lumb WV. A dorsolateral muscle-separating approach for thoracolumbar intervertebral disk fenestration in the dog. J Am Vet Med Assoc 1973;162(12):1037–40.

[5] Fingeroth JM. Fenestration. Pros and cons. Probl Vet Med 1989;1(3):445–66.

[6] Forterre F, Konar M, Spreng D, Jaggy A, Lang J. Influence of intervertebral disc fenestration at the herniation site in association with hemilaminectomy on recurrence in chondrodystrophic dogs with thoracolumbar disc disease: a prospective MRI study. Vet Surg 2008;37(4):399–405.

[7] Mayhew PD, McLear RC, Ziemer LS, Culp WT, Russell KN, Shofer FS, Kapatkin AS, Smith GK. Risk factors for recurrence of clinical signs associated with thoracolumbar intervertebral disk herniation in dogs: 229 cases (1994–2000). J Am Vet Med Assoc 2004;225(8):1231–6.

[8] Brisson BA, Moffatt SL, Swayne SL, Parent JM. Recurrence of thoracolumbar intervertebral disk extrusion in chondrodystrophic dogs after surgical decompression with or without prophylactic fenestration: 265 cases (1995–1999). J Am Vet Med Assoc 2004;224(11):1808–14.

[9] Wolgin M, Finkenberg J, Papaioannou T, Segil C, Soma C, Grundfest W. Excimer ablation of human intervertebral disc at 308 nanometers. Lasers Surg Med 1989;9(2):124–31.

[10] Dickey DT, Bartels KE, Henry GA, Stair EL, Schafer SA, Fry TR, Nordquist RE. Use of the holmium yttrium aluminum garnet laser for percutaneous thoracolumbar intervertebral disk ablation in dogs. J Am Vet Med Assoc 1996;208(8):1263–7.

[11] Bartels KE, Higbee RG, Bahr RJ, Galloway DS, Healey TS, Arnold C. Outcome of and complications associated with prophylactic percutaneous laser disk ablation in dogs with thoracolumbar disk disease: 277 cases (1992–2001). J Am Vet Med Assoc 2003;222(12):1733–9.

[12] Yasuma T, Makino E, Saito S, Inui M. Histological development of intervertebral disc herniation. J Bone Joint Surg Am 1986;68(7):1066–72.

[13] Lyons G, Eisenstein SM, Sweet MB. Biochemical changes in intervertebral disc degeneration. Biochim Biophys Acta 1981;673(4):443–53.

[14] Lee R. Interpretation of radiographs: inter-vertebral disc lesions in the dog. J Small Anim Pract 1973;14(2):111–2.

[15] Stigen Ø, Kolbjørnsen Ø. Calcification of intervertebral discs in the dachshund: a radiographic and histopathologic study of 20 dogs. Acta Vet Scand 2007;49:39.

[16] Meij BP, Bergknut N. Degenerative lumbosacral stenosis in dogs. Vet Clin North Am Small Anim Pract 2010;40(5):983–1009.

[17] Antoniou J, Pike GB, Steffen T, Baramki H, Poole AR, Aebi M, et al. Quantitative magnetic resonance imaging in the assessment of degenerative disc disease. Magn Reson Med 1998;40(6):900–7.

[18] Jöbsis FF. Noninvasive, infrared monitoring of cerebral and myocardial oxygen sufficiency and circulatory parameters. Science 1977;198(4323):1264–7.

[19] El-Desoky AE, Seifalian A, Cope M, Delpy D, Davidson B. Changes in tissue oxygenation of the porcine liver measured by near-infrared spectroscopy. Liver Transpl Surg 1999;5(3):219–26.

[20] Gurjar RS, Backman V, Perelman LT, Georgakoudi I, Badizadegan K, Itzkan I, Dasari RR, Feld MS. Imaging human epithelial properties with polarized light-scattering spectroscopy. Nat Med 2001;7(11):1245–8.

[21] Mourant JR, Hielscher AH, Eick AA, Johnson TM, Freyer JP. Evidence of intrinsic differences in the light scattering

properties of tumorigenic and nontumorigenic cells. Cancer 1998;84(6):366–74.

[22] Bigio IJ, Mourant JR. Ultraviolet and visible spectroscopies for tissue diagnostics: fluorescence spectroscopy and elastic-scattering spectroscopy. Phys Med Biol 1997;42(5): 803–14.

[23] De Blasi RA, Quaglia E, Gasparetto A, Ferrari M. Muscle oxygenation by fast near infrared spectrophotometry (NIRS) in ischemic forearm. Adv Exp Med Biol 1992;316:163–72.

[24] Mourant JR, Canpolat M, Brocker C, Esponda-Ramos O, Johnson TM, Matanock A, Stetter K, Freyer JP. Light scattering from cells: the contribution of the nucleus and the effects of proliferative status. J Biomed Opt 2000;5(2):131–7.

[25] Kanick SC, van der Leest C, Aerts JG, Hoogsteden HC, Kascáková S, Sterenborg HJ, Amelink A. Integration of single-fiber reflectance spectroscopy into ultrasound-guided endoscopic lung cancer staging of mediastinal lymph nodes. J Biomed Opt 2010;15(1):017004.

[26] Yu B, Burnside ES, Sisney GA, Harter JM, Zhu C, Dhalla AH, Ramanujam N. Feasibility of near-infrared diffuse optical spectroscopy on patients undergoing imageguided core-needle biopsy. Opt Express 2007;15(12):7335–50.

[27] Radhakrishnan H, Senapati A, Kashyap D, Peng YB, Liu H. Light scattering from rat nervous system measured intraoperatively by near-infrared reflectance spectroscopy. J Biomed Opt 2005;10(5):051405.

[28] Bevilacqua F, Depeursinge C. Monte Carlo study of diffuse reflectance at source-detector separations close to one transport mean free path. J Opt Soc Am A 1999;16(12):2935–45.

[29] Mourant JR, Bigio IJ, Jack DA, Johnson TM, Miller HD. Measuring absorption coefficients in small volumes of highly scattering media: source-detector separations for which path lengths do not depend on scattering properties. Appl Opt 1997;36(22):5655–61.

[30] Nachabé R, Hendriks BH, van der Voort M, Desjardins AE, Sterenborg HJ. Estimation of biological chromophores using diffuse optical spectroscopy: benefit of extending the UV-VIS wavelength range to include 1000 to 1600 nm. Biomed Opt Express 2010;1(5):1432–42.

[31] Kanick SC, Robinson DJ, Sterenborg HJ, Amelink A. Monte Carlo analysis of single fiber reflectance spectroscopy: photon path length and sampling depth. Phys Med Biol 2009;54(22):6991–7008.

[32] Kanick SC, Sterenborg HJ, Amelink A. Empirical model of the photon path length for a single fiber reflectance spectroscopy device. Opt Express 2009;17(2):860–71.

[33] Kanick SC, Gamm UA, Schouten M, Sterenborg HJ, Robinson DJ, Amelink A. Measurement of the reduced scattering coefficient of turbid media using single fiber reflectance spectroscopy: fiber diameter and phase function dependence. Biomed Opt Express 2011;2(6):1687–702.

[34] Martelli F, Zaccanti G. Calibration of scattering and absorption properties of a liquid diffusive medium at NIR wavelengths. CW method. Opt Express 2007;15(2):486–500.

[35] Wang X, Pogue BW, Jiang S, Dehghani H, Song X, Srinivasan S, et al. Image reconstruction of effective Mie scattering parameters of breast tissue in vivo with near-infrared tomography. J Biomed Opt 2006;11(4):041106.

[36] van Staveren HJ, Moes CJ, van Marie J, Prahl SA, van Gemert MJ. Light scattering in Intralipid-10% in the wavelength range of 400–1100 nm. Appl Opt 1991;30(31):4507–14.

[37] Lim C, Kweon OK, Choi MC, Choi J, Yoon J. Computed tomographic characteristics of acute thoracolumbar intervertebral disc disease in dogs. J Vet Sci 2010;11(1):73–9.

[38] Vorwerk D, Husemann T, Blazek V, Zolotas G, Günther RW. Laser ablation of the nucleus pulposus: optical properties of degenerated intervertebral disk tissue in the wavelength range 200 to 2200 nm. Rofo 1989;151(6):725–8.

[39] Beuthan J, Minet O, Müller G. Optical biopsy of cytokeratin and NADH in the tumor border zone. Ann N Y Acad Sci 1998;838:150–70.

Received December 2, 2011; revised February 10, 2012; accepted March 9, 2012